First detection of a key intermediate in the oxidation of fuel + NO systems: HONO

Lorena Marrodán,[†] Yu Song,[‡] Olivier Herbinet,[‡*] Maria U. Alzueta,[†] Christa Fittschen[‡], Yiguang Ju[♣] and Frédérique Battin-Leclerc[‡]

[†] Aragón Institute of Engineering Research (I3A), Department of Chemical and Environmental Engineering, University of Zaragoza, C/Mariano Esquillor s/n, Zaragoza 50018, Spain.

[‡] Laboratoire Réactions et Génie de Procédés, CNRS – Université de Lorraine, ENSIC, 1 rue Grandville, 54000 Nancy, France

[‡] Université Lille, CNRS, UMR 8522 - PC2A - Physicochimie des Processus de Combustion et de l'Atmosphère, F-59000 Lille, France

[♣] Department of Mechanical and Aerospace Engineering, Princeton University, NJ 08544, USA

Abstract:

This paper reports the first online gas phase detection of absolute concentrations of HONO under engine relevant conditions, during the oxidation of an alkane in the presence of NO_x. The detection was achieved at laboratory scale thanks to the coupling of a jet-stirred reactor to a continuous-wave Cavity Ring-Down Spectroscopy cell. The evidence of the formation of HONO was obtained by comparing measured cw-CRDS spectra with a literature one. The formation of HONO was simultaneously observed with the appearance of another nitrogen compound: NO_2. This confirms that HONO could also be formed from NO_2 under engine conditions.

* Olivier Herbinet, Associate Professor at the University of Lorraine
e-mail: olivier.herbinet@univ-lorraine.fr
tel: +33 (0)3 72 74 38 22

1. Introduction

Nitrous acid (HONO) is a key species in the atmosphere because it contributes to its oxidizing capacity. The photolysis of HONO in many environments is a significant source of OH radicals during daytime [1–4]. The absorption spectrum of HONO extends well into the actinic range, making HONO an important source for OH radicals indoor [5]. The heterogeneous conversion of NO_2 is thought to be a major HONO source at nighttime as well as indoors [6,7]. However, the detailed analysis of field campaign data reveals that HONO formation paths are far from being understood and major HONO sources are still to be discovered [8,9]. Another possible source for HONO is the direct emission in the exhaust gases from internal combustion engines [10]. The detection of this species in exhaust gases was so far not directly performed in the gas phase, but in the liquid phase after absorption of HONO in water forming nitrite ions [10]. The formation of this intermediate is considered in gas phase detailed kinetic models [11] but, to our knowledge, it has not yet been directly measured in gas phase under conditions relevant to engines.

Under engine conditions, HONO may have a significant impact on the ignition process, since HONO rapidly dissociates to NO and highly reactive OH radicals. In conventional internal combustion engines, low amount of NO_2 is mainly formed from NO, after fuel oxidation, via the reactions of peroxy radicals (ROO in Figure 1) and NO to RO + NO_2 and subsequent reactions between NO_2 and intermediate species. However, two recent directions for engine improvement, such as exhaust gas recirculation [12] and the addition of alkyl-nitrates as additives to increase reactivity [13], introduce larger concentrations of NO_x in the fuel-air mixture prior to ignition. As reported by Chai and Goldsmith [14], the reaction between fuel (RH) and NO_2: $RH+NO_2 \rightarrow R+HONO$ is one reaction channel for HONO formation (Figure 1). Moreover, previous studies on the effects of NO addition during alkanes oxidation [15] reported another HONO reaction channel via $NO+OH+M \rightarrow HONO+M$ at low temperatures is a key chain-terminating reaction to inhibit reactivity. In this study, we report the importance of different HONO formation channels at engine relevant conditions via NO_2 reactions with intermediate species such as HO_2, CH_2O, CH_3O, and H_2O_2 (Figure 1). This formation pathways have never been proven under the above-mentioned conditions.

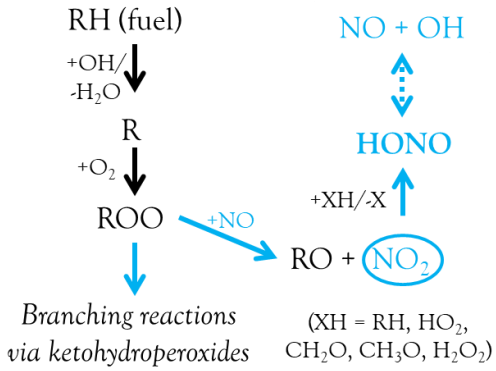

Figure 1: Main formation and consumption pathways of HONO and NO_2.

HONO has been previously detected in atmospheric chemistry studies by different spectroscopic methods in the UV-vis [16], IR [17], and near IR ranges [18]. Obtaining absorption cross sections, indispensable for a quantitative detection, is however not straightforward in spectroscopic measurements, because HONO exists in equilibrium with other N-compounds such as NO, NO_2 or HNO_3. Jain et al. [18] solved this problem by generating HONO in-situ and deducing its concentration from time-resolved traces taking advantage of well-known rate constants. In the atmosphere, HONO has also been measured thanks to an in situ instrument, LOPAP (long path absorption photometer), using a wet chemical sampling followed by a photometric detection [19].

The purpose of this work is to accurately quantify HONO under conditions relevant to internal combustion engines using online sampling in the gas phase followed by a quantification using cw-CRDS. Oxidation experiments were performed using *n*-pentane, one of the smallest alkanes having a significant reactivity at low temperature (below 800 K), the temperature range where HONO concentration is significant according to detailed kinetic models.

2. Experimental method

Pulsed cavity ring-down spectroscopy invented in 1988 [20] consists of measuring the decay time of a light pulse trapped within a cavity. Measuring this decay time as a function of the wavelength allows identifying and quantifying trace species. Pulsed CRDS has been used in the area of combustion since the mid 90s to detect various intermediates [21]. The more complex CRDS variant using a continuous wave laser (cw-CRDS) provides higher sensitivity, repetition rates and spectral resolution. A scheme of the cw-CRDS cell used in the present work is displayed in Figure 2. A complete description of the setup

has been published earlier [22] and can be found as supplementary material. The cw-CRDS cell consists of a glass tube with an inner diameter of 6 mm and a length of 80 cm. The gas is pumped from the JSR through a quartz probe with a small orifice into this cell at a flow rate of about 300 cm^3 min^{-1}. Following this expansion, the gas is at ambient temperature and the pressure is around 1.33 kPa (10 Torr). Two highly reflective mirrors (with a reflectivity of around 0.9999) are mounted at each end of the cell (one of them is fixed to a piezo to vary the length of the cavity around an equilibrium position and obtains the cavity resonance, characterized by a strong emission from the cavity). The laser light is provided by a diode laser emitting in the range 6624-6647 cm^{-1}. The diode laser emission is directly fibred and passes through a fibred optical isolator and a fibred acousto-optical modulator which allows the laser beam to be deviated when the resonance occurs (detected by the strong emission from the cavity). The optical signal transmitted through the cavity is converted into the electric current by an avalanche photodiode and the ring-down time τ is obtained by fitting the exponential decay over a time range of seven lifetimes by a Levenberg-Marquardt exponential fit (see SM for additional details about this setup).

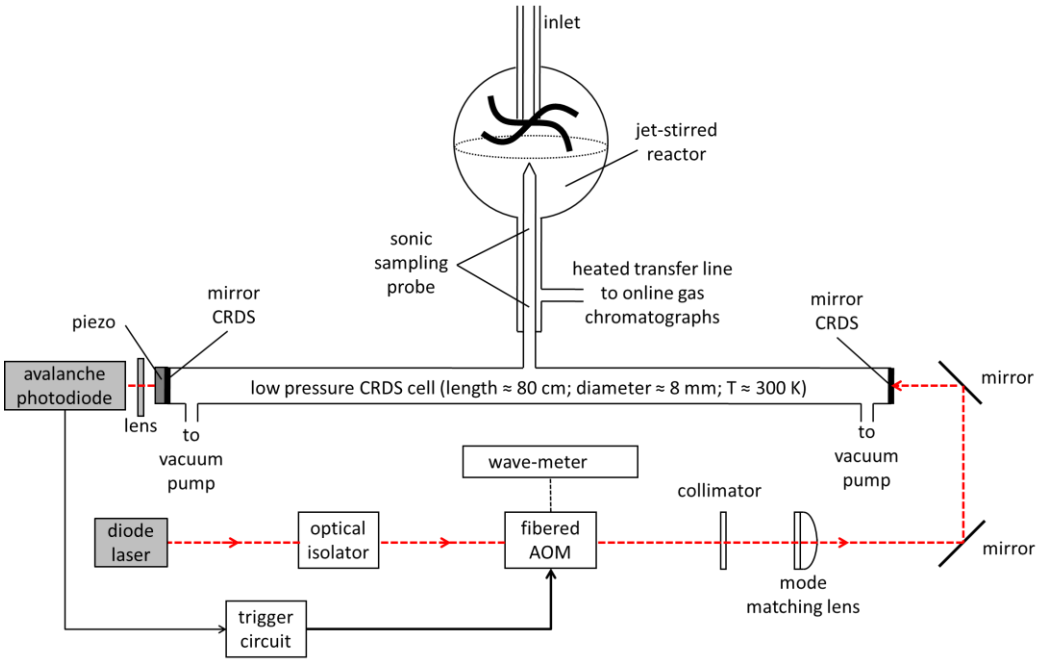

Figure 2: Scheme of the JSR and cw-CRDS setup.

The reaction takes place in a fused silica jet-stirred reactor, a type of continuous stirred tank reactor operated under steady state and characterized by homogenous gas phase composition and temperature. This reactor has been used for numerous oxidation and pyrolysis gas phase kinetic studies [23]. The direct sampling of the reactor gas phase is performed using a fused silica sonic probe. This probe creates

the necessary pressure drop between the reactor working at a pressure of 106.7 kPa (800 Torr) and the spectroscopic cell under partial vacuum (1.33 kPa). It also cools down the sampled gas to quench any further reactions in the diagnostic part of the setup. The heating of the JSR is achieved thanks to Thermocoax resistances regulated using Eurotherm controllers and K-type thermocouples located between resistances and the reactor wall. The reaction temperature (±5 K) is measured at the center of the spherical reactor thanks to an additional K-type thermocouple inserted in the intra-annular part of the preheating zone used as a glass finger (a scheme is given in SM). Gas (argon, O_2 and NO) and liquid (*n*-pentane) flow rates are controlled with mass flow and Coriolis flow controllers provided by Bronkhorst, respectively (relative uncertainty of ±0.5%).

This setup has already successfully been used to perform the quantification of hydrogen peroxide (H_2O_2), a species for which mole fractions are usually not reported because of analytical difficulties related to the relative low stability of this species due to the weak O-O bond, in the oxidation under engine relevant conditions of various fuels, such as alkanes from *n*-butane to *n*-heptane, and some oxygenates such as dimethyl-ether and *n*-hexanal [24,22,25,26].

3. Experimental results

In the present experiments, HONO was detected during the oxidation of *n*-pentane in the presence of NO. The advantage of *n*-pentane is that it is reactive below 800 K [27], the temperature region were large HONO mole fractions are expected according to detailed kinetic models. The study was carried out over the temperature range 500 – 775 K, at a residence time of 2.0±0.1 s and pressure of 106.7 kPa. The inlet composition was a stoichiometric mixture of 10,000 ppm of *n*-pentane and 80,000 ppm of O_2, in the presence of 500 ppm of NO, with high dilution into argon (argon mole fraction of 0.9095 to close the balance). In addition to cw-CRDS, two other diagnostic tools were also used: gas chromatography for the quantification of carbon containing species and a NO_x analyzer for NO and NO_2 detection.

A first attempt of detecting HONO was performed during the oxidation of methane doped with NO and NO_2 [28]. However, HONO could not be detected during that study likely because HONO mole fractions were below the detection limit estimated as 3 ppm, which was in agreement with predictions using the detailed kinetic model developed in that work [28]. Even with the promoting effect of the

additions of NO or NO_2, methane oxidation starts above 800 K which is not favorable for HONO detection.

Figure 3a displays the mole fractions of *n*-pentane as a function of temperature measured using gas chromatography. To highlight the effect of the addition of NO on the reactivity, two profiles are displayed: one corresponding to the oxidation of neat *n*-pentane (red crosses), and one in the presence of 500 ppm NO (green circles).

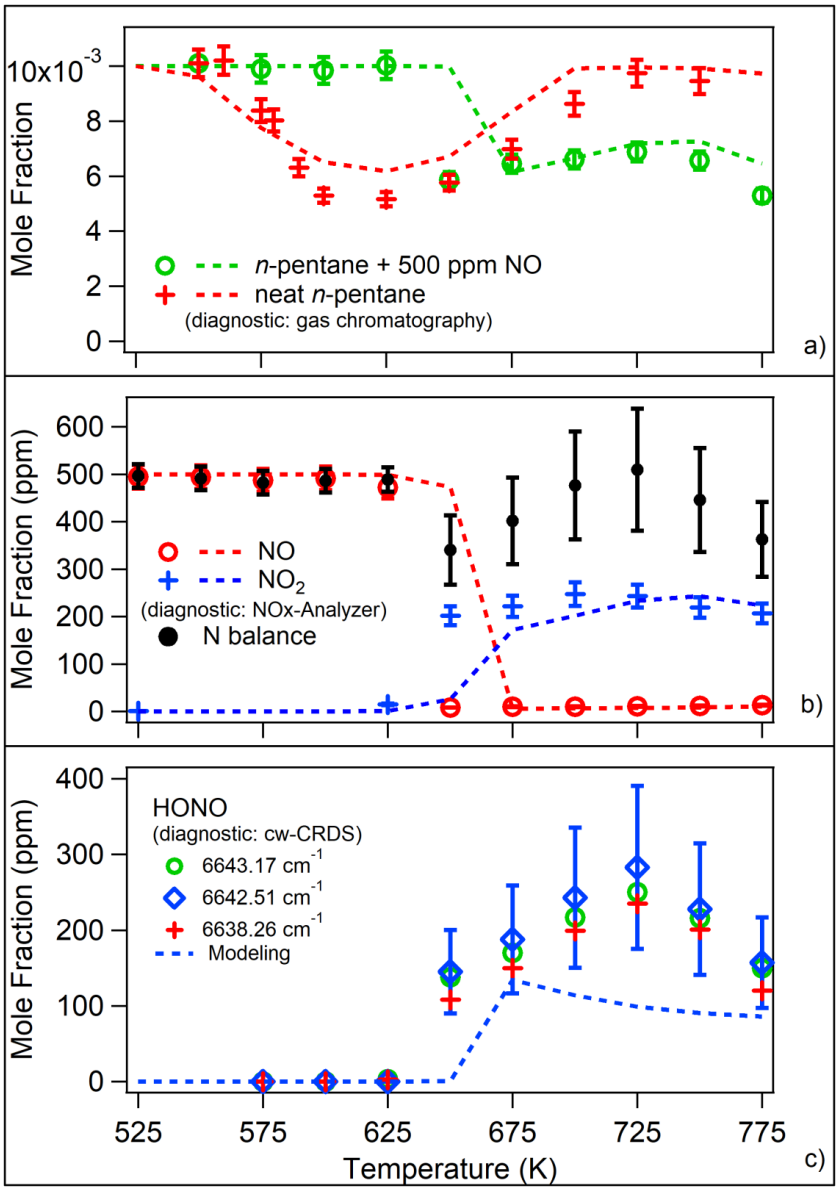

Figure 3. Mole fractions as a function of temperature of a) *n*-pentane with and without addition of 500 ppm NO, b) NO, NO_2 and N-atom balance c) HONO for the three selected cw-CRDS lines.

For the oxidation of neat *n*-pentane, the mole fraction temperature dependence exhibits the classical behavior observed for *n*-alkanes: a first reactivity zone indicating low-temperature chemistry, a marked negative temperature coefficient area, followed by a second reactivity zone corresponding to the high-temperature chemistry. The fuel mole fraction temperature dependence obtained in the presence of the 500 ppm of NO is quite different. It shows the antagonistic effect of NO on the oxidation of *n*-pentane: an inhibition of the reaction below 650 K and a reactivity enhancement above 650 K. The temperature dependence still exhibits a negative temperature coefficient area, but it is much less marked than for neat *n*-pentane.

A limited number of nitrogen containing products was detected during this study. These products are NO, NO_2 and HONO. The concentration profile of NO is displayed in Figure 3b. An abrupt consumption of NO is observed between 625 and 650 K. It corresponds to the temperature from which *n*-pentane consumption is observed in Figure 3a. As expected at such low temperatures, an important product from the oxidation of NO is NO_2 (Figure 1). The temperature dependence of the NO_2 concentration is also displayed in Figure 3b: NO_2 represents a little bit more than half of the consumed NO around 700 K. This indicates that other nitrogen containing species are formed.

Figure 4 displays the spectrum recorded using cw-CRDS during the oxidation of *n*-pentane + NO at 700 K. Strong evidence for the formation of HONO is shown by comparing this spectrum to a HONO spectrum recorded by Jain and coworkers [18]. Four main peaks are well visible on the literature spectrum over the range 6638 – 6643 cm^{-1}. These four peaks are also present in the spectrum recorded at 700 K. Moreover, the comparison shows an excellent agreement of both shapes and relative intensity for all four peaks. A large peak which cannot be attributed to absorption by HONO is also visible (at about 6641.0 cm^{-1}) in the spectrum recorded during this work. This peak is due to the presence of water, one of the main reaction products of fuel oxidation, which has several absorption lines in the wavelength range investigated in this study, as it can be seen in the water literature spectrum displayed in Figure 4. Other less intense peaks due to the absorption of light by water are well present (e.g., the peaks at 6638.9, 6641.3 and 6641.6 cm^{-1}).

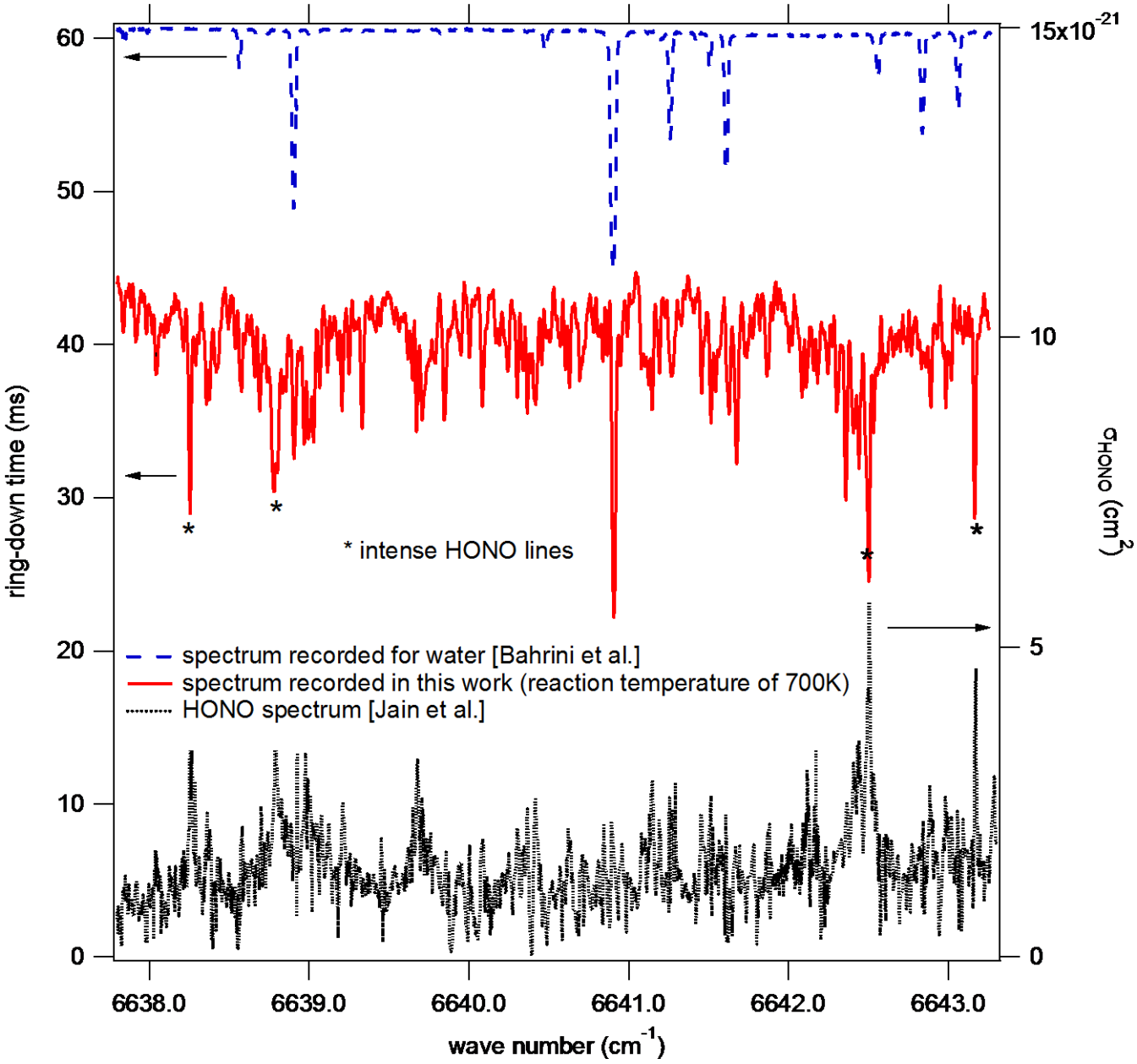

Figure 4. Comparison of the cw-CRDS spectrum obtained in the present study during the oxidation of *n*-pentane + NO at 700 K, the literature HONO spectrum recorded by Jain and coworkers [18], and that recorded for water by Bahrini et al. [29].

The quantification of HONO was performed at three different spectral lines at 6638.26, 6642.51 and 6643.17 cm^{-1} using the absorption cross-sections published by Jain and coworkers [18]. The quantification was also performed for the less intense line at 6637.36 cm^{-1} (in very good agreement with all other three sets of data) but is not shown for the clarity of the graph in Figure 3c (see Figure S3 in

SM for the quantification of all four lines). Absorption cross-sections and uncertainties are given in Table 1. Reported uncertainties are quite large, for the line at 6638.26 cm^{-1} it is 42%.

Table 1. Cross sections used for the quantification of HONO [18].

Wavenumber (cm^{-1})	Absorption cross-section (10^{-21} cm^2)
6638.26	3.8±1.6
6642.51	5.8±2.2
6643.17	4.2±1.7

The temperature dependence of HONO concentrations obtained from the analysis of the three lines are displayed in Figure 3c. The three lines provide data in excellent agreement. As for other products, an abrupt increase of the concentration is observed between 625 and 650 K. At 725 K, the temperature for which the HONO mole fraction is at the maximum, the average concentration of HONO is 256±24 ppm. Error bars have been drawn in the graph of Figure 3c considering the reported uncertainty for the line at 6642.51 cm^{-1} (the line for which the uncertainty is the lowest). The nitrogen atom balance (Figure 3b) shows that measured HONO concentrations are quite consistent at 725 K (the sum of the concentrations of NO, NO_2 and HONO is 510±128 ppm). N-balance deviations observed at lower and higher temperatures may indicate that one or several nitrogen containing species could be formed but not being detected.

The formation of many carbon containing reaction products was observed, as in our previous studies on neat alkanes [27], most of them being carbon containing species. These products are not discussed here as the current focus is on nitrogen containing products and particularly the detection of HONO. Mole fractions of all reaction products are given in SM.

4. Comparison with computed data

Model calculations included in Figure 3 were performed with a kinetic mechanism based on a *n*-pentane oxidation mechanism well validated under JSR conditions [27,30] and an updated NOx sub-mechanism [28]. Reactions to merge the *n*-pentane mechanism and the NO_x sub-mechanism, by analogy with *n*-pentane/*n*-butane and NO [14] and the work for the oxidation of engine surrogate fuels (*n*-heptane, *iso*-octane and toluene) in the presence of NO_x [15], were augmented in the model as

well. Moreover, the chemistry of HONO was also updated by the adoption of the available rate constant for NO+OH(+M)=HONO(+M) [31], along with a modified third-body coefficient for Ar (coefficient of 0.1), and HONO forming reaction (NO_2+HO_2=HONO+O_2) was adopted following Rasmussen et al. [32]. The reaction associated with OH radical attacking HONO to form NO_2 and H_2O was implemented with the aids of Burkholder et al. [33]. The complete mechanism (832 species and 4217 reactions) is provided as supplemental material of this paper in CHEMKIN format, along with thermodynamic properties.

In the absence of NO, the model predicts quite well the low-temperature behavior of the "*n*-pentane + O_2" system with the negative temperature coefficient phenomenon (Figure 3a). Model predictions are also in good agreement in the presence of NO with the shift of the onset of low temperature reactivity towards higher temperature and then a higher reactivity than in the absence of NO as in experiments. As far as nitrogen-containing species are concerned, the mole fractions of NO and NO_2 are satisfactorily predicted by the model, even if the consumption of NO and the increase of the model fraction of NO_2 are a little bit shifted of about 25 K. The order of magnitude of HONO concentrations is satisfactorily predicted by the model. Some deviations are observed between the computed and the experimental profiles. The model also predicts the formation of nitro-compounds like nitro-ethane, for example, but this type of species was not observed during experiments.

5. Conclusion

This study presents the first reliable direct quantification of HONO in the gas phase during the oxidation of a fuel in the presence of NO. The ability to detect this key intermediate adds an important constraint to the models to improve the understanding of the specific low-temperature oxidation chemistry of fuel – NO_x systems for further improvement of more efficient and cleaner combustion applications. This quantification confirms the role of exhaust gas emissions, as a HONO source, in the atmosphere. Moreover, it will favor the development of reliable chemical kinetic mechanisms to be used in constraint to the models of newly proposed engine types.

Acknowledgment

This work has received funding from the European Union H2020 (H2020-SPIRE-04-2016) under Grant agreement no. 723706 and from the COST Action CM1404 “Chemistry of smart energy carriers and technologies”. Ms. Marrodán acknowledges Aragón Government for the predoctoral grant awarded.

References

[1] J. Kleffmann, T. Gavriloaiei, A. Hofzumahaus, F. Holland, R. Koppmann, L. Rupp, E. Schlosser, M. Siese, A. Wahner, Daytime formation of nitrous acid: A major source of OH radicals in a forest, Geophysical Research Letters. 32 (2005). doi:10.1029/2005GL022524.

[2] H. Su, Y. Cheng, R. Oswald, T. Behrendt, I. Trebs, F.X. Meixner, M.O. Andreae, P. Cheng, Y. Zhang, U. Pöschl, Soil Nitrite as a Source of Atmospheric HONO and OH Radicals, Science. 333 (2011) 1616–1618. doi:10.1126/science.1207687.

[3] G. Villena, P. Wiesen, C.A. Cantrell, F. Flocke, A. Fried, S.R. Hall, R.S. Hornbrook, D. Knapp, E. Kosciuch, R.L. Mauldin, J.A. McGrath, D. Montzka, D. Richter, K. Ullmann, J. Walega, P. Weibring, A. Weinheimer, R.M. Staebler, J. Liao, L.G. Huey, J. Kleffmann, Nitrous acid (HONO) during polar spring in Barrow, Alaska: A net source of OH radicals?, Journal of Geophysical Research: Atmospheres. 116 (2011). doi:10.1029/2011JD016643.

[4] B. Aumont, F. Chervier, S. Laval, Contribution of HONO sources to the NOx/HOx/O3 chemistry in the polluted boundary layer, Atmospheric Environment. 37 (2003) 487–498. doi:10.1016/S1352-2310(02)00920-2.

[5] E. Gómez Alvarez, D. Amedro, C. Afif, S. Gligorovski, C. Schoemaecker, C. Fittschen, J.-F. Doussin, H. Wortham, Unexpectedly high indoor hydroxyl radical concentrations associated with nitrous acid, PNAS. 110 (2013) 13294–13299. doi:10.1073/pnas.1308310110.

[6] B.J. Finlayson-Pitts, L.M. Wingen, A.L. Sumner, D. Syomin, K.A. Ramazan, The heterogeneous hydrolysis of NO_2 in laboratory systems and in outdoor and indoor atmospheres: An integrated mechanism, Phys. Chem. Chem. Phys. 5 (2003) 223–242. doi:10.1039/B208564J.

[7] M. Mendez, N. Blond, D. Amedro, D.A. Hauglustaine, P. Blondeau, C. Afif, C. Fittschen, C. Schoemaecker, Assessment of indoor HONO formation mechanisms based on in situ measurements and modeling, Indoor Air. 27 (2017) 443–451. doi:10.1111/ina.12320.

[8] J.D. Lee, L.K. Whalley, D.E. Heard, D. Stone, R.E. Dunmore, J.F. Hamilton, D.E. Young, J.D. Allan, S. Laufs, J. Kleffmann, Detailed budget analysis of HONO in central London reveals a missing daytime source, Atmospheric Chemistry and Physics. 16 (2016) 2747–2764. doi:https://doi.org/10.5194/acp-16-2747-2016.

[9] H. Meusel, U. Kuhn, A. Reiffs, C. Mallik, H. Harder, M. Martinez, J. Schuladen, B. Bohn, U. Parchatka, J.N. Crowley, H. Fischer, L. Tomsche, A. Novelli, T. Hoffmann, R.H.H. Janssen, O. Hartogensis, M. Pikridas, M. Vrekoussis, E. Bourtsoukidis, B. Weber, J. Lelieveld, J. Williams, U. Pöschl, Y. Cheng, H. Su, Daytime formation of nitrous acid at a coastal remote site in Cyprus indicating a common ground source of atmospheric HONO and NO, Atmospheric Chemistry and Physics. 16 (2016) 14475–14493. doi:https://doi.org/10.5194/acp-16-14475-2016.

[10] H.T. Trinh, K. Imanishi, T. Morikawa, H. Hagino, N. Takenaka, Gaseous nitrous acid (HONO) and nitrogen oxides (NOx) emission from gasoline and diesel vehicles under real-world driving test cycles, Journal of the Air & Waste Management Association. 67 (2017) 412–420. doi:10.1080/10962247.2016.1240726.

[11] P. Dagaut, P. Glarborg, M.U. Alzueta, The oxidation of hydrogen cyanide and related chemistry, Progress in Energy and Combustion Science. 34 (2008) 1–46. doi:10.1016/j.pecs.2007.02.004.

[12] G.T. Kalghatgi, Developments in internal combustion engines and implications for combustion science and future transport fuels, Proceedings of the Combustion Institute. 35 (2015) 101–115. doi:10.1016/j.proci.2014.10.002.
[13] S.S. Goldsborough, M.V. Johnson, C. Banyon, W.J. Pitz, M.J. McNenly, Experimental and modeling study of fuel interactions with an alkyl nitrate cetane enhancer, 2-ethyl-hexyl nitrate, Proceedings of the Combustion Institute. 35 (2015) 571–579. doi:10.1016/j.proci.2014.06.048.
[14] J. Chai, C.F. Goldsmith, Rate coefficients for fuel+NO_2: Predictive kinetics for HONO and HNO_2 formation, Proceedings of the Combustion Institute. 36 (2017) 617–626. doi:10.1016/j.proci.2016.06.133.
[15] G. Moréac, P. Dagaut, J.F. Roesler, M. Cathonnet, Nitric oxide interactions with hydrocarbon oxidation in a jet-stirred reactor at 10 atm, Combustion and Flame. 145 (2006) 512–520. doi:10.1016/j.combustflame.2006.01.002.
[16] D. Perner, U. Platt, Detection of nitrous acid in the atmosphere by differential optical absorption, Geophysical Research Letters. 6 (1979) 917–920. doi:10.1029/GL006i012p00917.
[17] R.S. Karlsson, E.B. Ljungstrom, Laboratory study of ClNO: Hydrolysis, Environ. Sci. Technol. 30 (1996) 2008–2013. doi:10.1021/es950801f.
[18] C. Jain, P. Morajkar, C. Schoemaecker, B. Viskolcz, C. Fittschen, Measurement of Absolute Absorption Cross Sections for Nitrous Acid (HONO) in the Near-Infrared Region by the Continuous Wave Cavity Ring-Down Spectroscopy (cw-CRDS) Technique Coupled to Laser Photolysis, J. Phys. Chem. A. 115 (2011) 10720–10728. doi:10.1021/jp203001y.
[19] J. Heland, J. Kleffmann, R. Kurtenbach, P. Wiesen, A new instrument to measure gaseous nitrous acid (HONO) in the atmosphere, Environ. Sci. Technol. 35 (2001) 3207–3212. doi:10.1021/es000303t.
[20] A. O'Keefe, D.A.G. Deacon, Cavity ring- down optical spectrometer for absorption measurements using pulsed laser sources, Review of Scientific Instruments. 59 (1988) 2544–2551. doi:10.1063/1.1139895.
[21] X. Mercier, E. Therssen, J.F. Pauwels, P. Desgroux, Quantitative features and sensitivity of cavity ring-down measurements of species concentrations in flames, Combustion and Flame. 124 (2001) 656–667. doi:10.1016/S0010-2180(00)00230-3.
[22] C. Bahrini, P. Morajkar, C. Schoemaecker, O. Frottier, O. Herbinet, P.-A. Glaude, F. Battin-Leclerc, C. Fittschen, Experimental and modeling study of the oxidation of n-butane in a jet stirred reactor using cw-CRDS measurements, Phys. Chem. Chem. Phys. 15 (2013) 19686–19698. doi:10.1039/C3CP53335B.
[23] O. Herbinet, F. Battin-Leclerc, Progress in Understanding Low-Temperature Organic Compound Oxidation Using a Jet-Stirred Reactor, Int. J. Chem. Kinet. 46 (2014) 619–639. doi:10.1002/kin.20871.
[24] C. Bahrini, O. Herbinet, P.-A. Glaude, C. Schoemaecker, C. Fittschen, F. Battin-Leclerc, Quantification of Hydrogen Peroxide during the Low-Temperature Oxidation of Alkanes, J. Am. Chem. Soc. 134 (2012) 11944–11947. doi:10.1021/ja305200h.
[25] A. Rodriguez, O. Frottier, O. Herbinet, R. Fournet, R. Bounaceur, C. Fittschen, F. Battin-Leclerc, Experimental and Modeling Investigation of the Low-Temperature Oxidation of Dimethyl Ether, J. Phys. Chem. A. 119 (2015) 7905–7923. doi:10.1021/acs.jpca.5b01939.
[26] A. Rodriguez, O. Herbinet, F. Battin-Leclerc, A study of the low-temperature oxidation of a long chain aldehyde: n-hexanal, Proceedings of the Combustion Institute. 36 (2017) 365–372. doi:10.1016/j.proci.2016.05.047.
[27] J. Bugler, A. Rodriguez, O. Herbinet, F. Battin-Leclerc, C. Togbé, G. Dayma, P. Dagaut, H.J. Curran, An experimental and modelling study of n-pentane oxidation in two jet-stirred reactors: The importance of pressure-dependent kinetics and new reaction pathways, Proceedings of the Combustion Institute. 36 (2017) 441–448. doi:10.1016/j.proci.2016.05.048.
[28] Y. Song, L. Marrodán, N. Vin, O. Herbinet, E. Assaf, C. Fittschen, A. Stagni, T. Faravelli, M.U. Alzueta, F. Battin-Leclerc, The sensitizing effects of NO_2 and NO on methane low temperature ox-

idation in a jet stirred reactor, Proceedings of the Combustion Institute. (2018). doi:10.1016/j.proci.2018.06.115.
[29] C. Bahrini, O. Herbinet, P.-A. Glaude, C. Schoemaecker, C. Fittschen, F. Battin-Leclerc, Detection of some stable species during the oxidation of methane by coupling a jet-stirred reactor (JSR) to cw-CRDS, Chemical Physics Letters. 534 (2012) 1–7. doi:10.1016/j.cplett.2012.03.012.
[30] A. Rodriguez, O. Herbinet, Z. Wang, F. Qi, C. Fittschen, P.R. Westmoreland, F. Battin-Leclerc, Measuring hydroperoxide chain-branching agents during n-pentane low-temperature oxidation, Proceedings of the Combustion Institute. 36 (2017) 333–342. doi:10.1016/j.proci.2016.05.044.
[31] R. Atkinson, D.L. Baulch, R.A. Cox, J.N. Crowley, R.F. Hampson, R.G. Haynes, M.E. Jenkin, M.J. Rossi, J. Troe, Evaluated kinetic and photochemical data for atmospheric chemistry: Volume I - Gas phase reactions of O_x, HO_x, NO_x and SO_x species, Atmos. Chem. Phys. 4 (2004) 1461–1738.
[32] C.L. Rasmussen, J. Hansen, P. Marshall, P. Glarborg, Experimental measurements and kinetic modeling of CO/H2/O2/NOx conversion at high pressure, International Journal of Chemical Kinetics. 40 (2008) 454–480. doi:10.1002/kin.20327.
[33] J.B. Burkholder, A. Mellouki, R. Talukdar, A.R. Ravishankara, Rate coefficients for the reaction of OH with HONO between 298 and 373 K, International Journal of Chemical Kinetics. 24 (1992) 711–725. doi:10.1002/kin.550240805.